

Practical 3-splitting beyond Strang

Raymond J. Spiteri^{1,2*}, Arash Tavassoli^{1,3†}, Siqi Wei^{1,2†}
and Andrei Smolyakov³

^{1*}Department of Computer Science, University of Saskatchewan,
110 Science Place, Saskatoon, S7N 5K9, SK, Canada.

²Department of Mathematics and Statistics, University of
Saskatchewan, 106 Wiggins Road, Saskatoon, S7N 5E6, SK,
Canada.

³Department of Physics and Engineering Physics, University of
Saskatchewan, 116 Science Place, Saskatoon, S7N 5E2, SK,
Canada.

*Corresponding author(s). E-mail(s): spiteri@cs.usask.ca;

Contributing authors: art562@usask.ca; siqi.wei@usask.ca;
andrei.smolyakov@usask.ca;

[†]These authors contributed equally to this work.

Abstract

Operator splitting is a popular divide-and-conquer strategy for solving differential equations. Typically, the right-hand side of the differential equation is split into a number of parts that can then be integrated separately. Many methods are known that split the right-hand side into two parts. This approach is limiting, however, and there are situations when 3-splitting is more natural and ultimately more advantageous. The second-order Strang operator-splitting method readily generalizes to a right-hand side splitting into any number of operators. It is arguably the most popular method for 3-splitting because of its efficiency, ease of implementation, and intuitive nature. Other 3-splitting methods exist, but they are less well-known, and evaluations of their performance in practice are scarce. We demonstrate the effectiveness of some alternative 3-split, second-order methods to Strang splitting on two problems: the reaction-diffusion Brusselator, which can be split into three parts that each have closed-form solutions, and the kinetic

Vlasov–Poisson equations that is used in semi-Lagrangian plasma simulations. We find alternative second-order 3-operator-splitting methods that realize efficiency gains of 10%–20% over traditional Strang splitting.

Keywords: operator-splitting methods, fractional-step methods, Brusselator, Vlasov–Poisson equations

1 Introduction

The mathematical modeling of the evolution of natural systems is commonly performed by means of differential equations. These differential equations often have contributions from distinct physical processes. In such cases, it has proven to be computationally fruitful to treat the individual terms (or *operators*) separately, i.e., by splitting methods. Different integrators can be used that take advantage of the specific properties of the individual operators. For example, implicit-explicit (IMEX) methods split the right-hand side into two operators, ideally one stiff and one non-stiff, and treat them with an implicit and an explicit method, respectively [1]. When the right-hand side consists of contributions from many processes, however, IMEX methods can suffer from the challenge of how to split the right-hand side into only two operators. In this study, we consider two systems, the Brusselator system [2] and the Vlasov–Poisson equations, that admit useful 3-splittings.

Because they are less frequently used, 3-splitting methods are less well known than 2-splitting methods. The well-known second-order Strang–Marchuk (or simply *Strang*) splitting method [3, 4] admits an intuitive generalization to any number of operators, and because of this, it is arguably the most popular 3-splitting method. Other 3-splitting methods can be derived by considering the order conditions of the splitting method together with favorable properties such as symmetry and local error minimization [5, 6]. Moreover, adaptive 3-splitting methods and 3-splitting methods with complex coefficients are proposed in [6]. These 3-splitting methods are less well-known, less intuitive, and their performance in practice has not been widely studied.

In [7], the authors compared an adaptive third-order 2-splitting method PP 3/4 A c [6] with an adaptive third-order 3-splitting method PP 3/4 A 3 c [6] applied to the Gray–Scott equations. They concluded that although the 3-splitting method requires fewer steps for a given accuracy, the additional computation cost required per step ultimately led to underperformance.

For some problems, however, a 3-splitting method can lead to more operators that have a closed-form solution that can be evaluated efficiently. In [8], the Vlasov–Maxwell system is split into three parts based on its Hamiltonian. Although this splitting allowed them to solve two parts exactly in time, the rotation part was solved approximately, using the Strang splitting. This approach is revisited in [9], where the authors split the Vlasov–Maxwell equations into three parts again, but instead of approximating the rotation

operator with a Strang splitting method, they developed a new splitting method to solve the rotation part exactly in time. Therefore, the three parts of the Vlasov–Maxwell system are solved exactly in time, significantly reducing the error of the overall solution and decreasing the computational cost compared to using a 2D interpolation. They also applied several 3-splitting methods of order 2, 3, 4, 6 to the Vlasov–Maxwell system, including AK 3-2(ii) and AK 5-2 from [6]. For 3-splitting methods of order two, the authors observed that AK 3-2(ii) generates the smallest error and hence is the most efficient second-order method.

The goal of this paper is to examine the performance in terms of overall computation efficiency of alternatives to Strang splitting for problems that lend themselves well to 3-splitting. A key observation is that although some second-order methods may yield smaller errors for a given step size, their additional computational cost per step may negate their overall efficiency.

The outline of the remainder of the paper is as follows. Some general theoretical background on operator splitting methods along with the specific operator-splitting methods considered in this study are given in sect. 2. Descriptions of the problems used to illustrate the performance of the methods follow in sect. 3, and the performance results themselves appear in sect. 4. Finally, some discussion and conclusions of the study are given in sect. 5.

2 Theoretical Background

In this section, we present some background on operator-splitting methods as discussed in [10], with a focus on 3-splitting methods.

Consider the initial-value problem (IVP) for an N -additively split ordinary differential equation

$$\frac{d\mathbf{y}}{dt} = \mathcal{F}(t, \mathbf{y}) = \sum_{\ell=1}^N \mathcal{F}^{[\ell]}(t, \mathbf{y}), \quad \mathbf{y}(0) = \mathbf{y}_0. \quad (1)$$

Let $\varphi_{\Delta t}^{[\ell]}$ be the flow of the sub-system

$$\frac{d\mathbf{y}^{[\ell]}}{dt} = \mathcal{F}^{[\ell]}(t, \mathbf{y}^{[\ell]}) \quad (2)$$

for $\ell = 1, 2, \dots, N$. Compositions of $\varphi_{\Delta t}^{[\ell]}$ can be used to construct numerical solutions to (1). For example, the following two methods

$$\Phi_{\Delta t} := \varphi_{\Delta t}^{[N]} \circ \varphi_{\Delta t}^{[N-1]} \circ \dots \circ \varphi_{\Delta t}^{[1]}, \quad (3a)$$

$$\Phi_{\Delta t}^* := \varphi_{\Delta t}^{[1]} \circ \varphi_{\Delta t}^{[2]} \circ \dots \circ \varphi_{\Delta t}^{[N]} \quad (3b)$$

are commonly known as the Godunov (or Lie–Trotter) splitting methods. The two methods (3a) and (3b) are adjoints of each other and are both first-order

4 Practical 3-splitting

accurate. Moreover, the flows $\left\{\varphi_{\Delta t}^{[\ell]}\right\}_{\ell=1}^N$ can be composed in any order to create a first-order accurate Godunov splitting method $\Phi_{\Delta t}^G$, and its adjoint $\Phi_{\Delta t}^{G*}$ can be derived by reversing the order of composition.

Another popular method is the Strang splitting method, which is constructed by composing $\Phi_{\Delta t}^G$ and $\Phi_{\Delta t}^{G*}$ with halved step sizes. Using (3a) and (3b), we can write a Strang splitting method as

$$\begin{aligned}\Psi_{\Delta t}^S &= \Phi_{\Delta t/2}^{G*} \circ \Phi_{\Delta t/2}^G \\ &= \varphi_{\Delta t/2}^{[1]} \circ \varphi_{\Delta t/2}^{[2]} \circ \cdots \circ \varphi_{\Delta t/2}^{[N-1]} \circ \varphi_{\Delta t}^{[N]} \circ \varphi_{\Delta t/2}^{[N-1]} \circ \cdots \circ \varphi_{\Delta t/2}^{[1]}.\end{aligned}\quad (4)$$

We note that the terms $\varphi_{\Delta t/2}^{[N]} \circ \varphi_{\Delta t/2}^{[N]}$ can be combined together as $\varphi_{\Delta t}^{[N]}$ by group property if $\varphi_{\Delta t/2}^{[N]}$ is the exact flow. If $\varphi_{\Delta t/2}^{[N]}$ is approximated, however, these two methods are different numerical methods with different accuracy and stability properties.

We express the general form of an s -stage operator-splitting methods as follows. Let $\alpha = [\alpha_1, \alpha_2, \dots, \alpha_s]$, where $\alpha_k = [\alpha_k^{[1]}, \alpha_k^{[2]}, \dots, \alpha_k^{[N]}]$, $k = 1, 2, \dots, s$, be coefficients of an operator-splitting method. An s -stage operator-splitting method that solves (1) can be written as

$$\Psi_{\Delta t} := \prod_{k=1}^s \Phi_{\alpha_k \Delta t}^{\{k\}} = \Phi_{\alpha_s \Delta t}^{\{s\}} \circ \Phi_{\alpha_{s-1} \Delta t}^{\{s-1\}} \circ \cdots \circ \Phi_{\alpha_1 \Delta t}^{\{1\}}, \quad (5)$$

where $\Phi_{\alpha_k \Delta t}^{\{k\}} := \varphi_{\alpha_k^{[N]} \Delta t}^{[N]} \circ \varphi_{\alpha_k^{[N-1]} \Delta t}^{[N-1]} \circ \cdots \circ \varphi_{\alpha_k^{[1]} \Delta t}^{[1]}$.

Henceforth, we focus on 3-splitting methods; i.e., $N = 3$. For the numerical method (5) to have order p_{OS} , the operator-splitting coefficients α must satisfy a system of order conditions in the form of polynomial equations. These equations can be derived from the well-known Baker–Campbell–Hausdorff (BCH) formula; see, e.g., [10]. The approach for deriving operator-splitting methods described in [11] also relies on the BCH formula, but the order conditions are generated automatically via computer algebra. Because our focus is on examining alternatives to Strang splitting with 3 operators, we focus on order conditions up to $p_{OS} = 2$ for the 3-splitting case:

$$p_{OS} = 1 : \quad \sum_{k=1}^s \alpha_k^{[1]} = 1, \quad \sum_{k=1}^s \alpha_k^{[2]} = 1, \quad \sum_{k=1}^s \alpha_k^{[3]} = 1, \quad (6a)$$

$$p_{OS} = 2 : \quad \sum_{k=1}^s \alpha_k^{[1]} \left(\sum_{k'=k}^s \alpha_{k'}^{[2]} \right) = \frac{1}{2}, \quad \sum_{k=1}^s \alpha_k^{[1]} \left(\sum_{k'=k}^s \alpha_{k'}^{[3]} \right) = \frac{1}{2}, \quad \sum_{k=1}^s \alpha_k^{[2]} \left(\sum_{k'=k}^s \alpha_{k'}^{[3]} \right) = \frac{1}{2} \quad (6b)$$

In this study, we are specifically interested in applications where the subsystems (2) can be solved exactly or with high precision. That is, the main source of error in the numerical solution is the splitting error. In [11], the authors developed a local error measure (LEM) based on the operator-splitting

coefficients α . Four second-order 3-splitting methods are proposed in [6]. They are Strang, AK 3-2(i), AK 3-2(ii), and AK 5-2. The efficiency of an operator-splitting method is affected by both the number of sub-integrations required by the method and (to some extent) by the LEM. To compare with Strang, we consider the class of three-stage, second-order 3-splitting methods denoted by OS 32-3. To satisfy the order conditions (6a) and (6b), an OS 32-3 method requires at least 5 sub-integrations. It is easy to show that all OS 32-3 methods that require exactly 5 sub-integrations are equivalent to Strang with different permutations of the operators ℓ . AK 3-2(i) is the OS 32-3 method with the smallest LEM for 6 sub-integrations. We constructed an OS 32-3 method with the smallest LEM that requires 7 sub-integrations and denote this method by OS 32-3(7). Table 1 summarizes the main characteristics of these five methods. The operator-splitting coefficients of AK 3-2(i), OS 32-3(7), AK 3-2(ii), and AK 5-2 are given in table 2, table 3, table 4, and table 5, respectively.

Method	Stages	Sub-integrations	LEM
Strang	3	5	1.48
AK 3-2(i)	3	6	1.06
OS 32-3(7)	3	7	0.30
AK 3-2(ii)	3	9	0.29
AK 5-2	5	9	0.22

Table 1 Summary of second-order 3-splitting methods considered.

k	$\alpha_1^{[k]}$	$\alpha_2^{[k]}$	$\alpha_3^{[k]}$
1	0.5	$1 - 1/\sqrt{2}$	$1/\sqrt{2}$
2	0	$1/\sqrt{2}$	$1 - 1/\sqrt{2}$
3	0.5	0	0

Table 2 Operator-splitting coefficients of AK 3-2(i)

k	$\alpha_1^{[k]}$	$\alpha_2^{[k]}$	$\alpha_3^{[k]}$
1	0.306975546320853	0.306975546320853	0.721475263023673
2	0	0.414499716702820	0
3	0.693024453679147	0.278524736976327	0.278524736976327

Table 3 Operator-splitting coefficients of OS 32-3(7)

3 Problem Descriptions

In this section, we describe two problems used to illustrate the performance of the second-order 3-splitting methods described in sect. 3. The first problem is the well-known Brusselator equation [2], which is a set of reaction-diffusion PDEs that describes an autocatalytic reaction between two chemical species

6 *Practical 3-splitting*

k	$\alpha_1^{[k]}$	$\alpha_2^{[k]}$	$\alpha_3^{[k]}$
1	0.316620935432115636	0.273890572734778059	0.662265355057626845
2	-0.0303736077786568570	0.438287559165397521	0.0664399910533392230
3	0.713752672346541221	0.287821868099824420	0.271294653889033932

Table 4 Operator-splitting coefficients of AK 3-2(ii)

k	$\alpha_1^{[k]}$	$\alpha_2^{[k]}$	$\alpha_3^{[k]}$
1	0.161862914279624	0.242677859055102	0.5
2	0.338137085720376	0.514644281889796	0
3	0.338137085720376	0	0.5
4	0	0.242677859055102	0
5	0.161862914279624	0	0

Table 5 Operator-splitting coefficients of AK 5-2

with different rates of diffusion. It is a commonly used benchmark problem for numerical methods because it exhibits interesting dynamics such as periodic solutions and bifurcations that are well understood analytically.

The second problem involves simulation of the electron cyclotron drift instability (ECDI) from the field of plasma physics. The ECDI is a plasma instability that is driven by the relative drift velocity of ions and electrons in the presence of a magnetic field. A number of factors, including high dimension, high resolution requirements, large required simulation domains, and long required simulation times, conspire to make this a challenging numerical problem. Simulations that provide meaningful data typically take on the order of ten days to run using 32 cores (with 80% scaling efficiency). Efficient time integration methods greatly impact such problems, where savings of 10%–20% translate to days or weeks of CPU time.

To measure the overall efficiency gain of a splitting method Ψ against the Strang splitting method, we should consider not only the total number of time steps required by each method but also the cost per step. Let N^S and $\hat{\tau}^S$ (N^Ψ and $\hat{\tau}^\Psi$) be the numbers of time steps and the wall clock times per time step of the Strang (Ψ) splitting method. The efficiency gain η of a splitting method Ψ with respect to Strang splitting is defined in terms of work-precision as

$$\eta := \frac{\tau^S - \tau^\Psi}{\tau^S},$$

where τ^S and τ^Ψ are the total wall clock time taken by the Strang and Ψ splitting methods, respectively. Hence,

$$\eta = \frac{N^S \hat{\tau}^S - N^\Psi \hat{\tau}^\Psi}{N^S \hat{\tau}^S} = 1 - \frac{N^\Psi \hat{\tau}^\Psi}{N^S \hat{\tau}^S} = 1 - \frac{\Delta t^S \hat{\tau}^\Psi}{\Delta t^\Psi \hat{\tau}^S}, \quad (7)$$

where Δt^S and Δt^Ψ are the largest step sizes for Strang and Ψ splitting method to achieve certain accuracy, respectively. The ratio $\frac{\hat{\tau}^\Psi}{\hat{\tau}^S}$ can be estimated using

the cost of additional sub-integrations required by performing Ψ compared with Strang. As indicated in sect. 2, the Strang splitting method requires $k^S = 5$ sub-integrations. Let k^Ψ be the number of sub-integrations required by the Ψ splitting method, then

$$\begin{aligned} \frac{\tilde{\tau}^\Psi}{\tilde{\tau}^S} &= \frac{\tilde{\tau}^S + \sum_{j=1}^{k^\Psi - k^S} \tilde{\tau}_j^\Psi}{\tilde{\tau}^S}, \\ &= 1 + \sum_{j=1}^{k^\Psi - k^S} \frac{\tilde{\tau}_j^\Psi}{\tilde{\tau}^S}, \end{aligned} \quad (8)$$

where $\tilde{\tau}_j^\Psi$ is the wall clock time of additional sub-integration j . We note that with this formula, we have taken into account that the cost of solving each operator can be different. Now we define the ratio $\delta := \frac{\Delta t^\Psi}{\Delta t^S}$ and the extra-time-fraction $\Gamma = \sum_{j=1}^{k^\Psi - k^S} \frac{\tilde{\tau}_j^\Psi}{\tilde{\tau}^S}$. Using (7) and (8), we can write η as

$$\eta = 1 - \frac{1 + \Gamma}{\delta}. \quad (9)$$

Some benchmarking studies consider the efficiency of a numerical method as its accuracy per time step [12, 13]. However, such approaches do not consider the computational cost of each step required to achieve a given accuracy. In other words, the accuracy per time step of two competing methods can be used to calculate δ , but it neglects the factor of Γ . Similarly, even if it were a perfect error estimator, the LEM does not include any information about the Γ factor. Therefore, it is not surprising that a particular method can be less efficient than another despite having a smaller LEM.

3.1 Brusselator

The Brusselator problem is a reaction-diffusion system that is commonly solved using 2-splitting method according to reaction and diffusion, e.g., [14]. When split into two operators, the reaction operator is non-linear and does not have a closed-form solution. In this study, we split the Brusselator problem into three operators. This splitting allows for a closed-form solution to each operator.

The Brusselator problem is defined as

$$\frac{\partial T}{\partial t} = D_1 \frac{\partial^2 T}{\partial x^2} + \alpha - (\beta + 1)T + T^2 C, \quad (10a)$$

$$\frac{\partial C}{\partial t} = D_2 \frac{\partial^2 C}{\partial x^2} + \beta T - T^2 C, \quad (10b)$$

8 *Practical 3-splitting*

where $T = T(x, t)$ and $C = C(x, t)$ represent concentrations of different chemical species. The parameter values are $\alpha = 0.6$, $\beta = 2$, and $D_1 = D_2 = \frac{1}{40}$, with boundary conditions $T(0, t) = T(1, t) = \alpha$ and $C(0, t) = C(1, t) = \frac{\beta}{\alpha}$ and initial conditions $T(x, 0) = \alpha + x(1 - x)$ and $C(x, 0) = \frac{\beta}{\alpha} + x^2(1 - x)$. Equation (10) is split into three parts as

$$\begin{cases} \frac{\partial T^{[1]}}{\partial t} = D_1 \frac{\partial^2 T^{[1]}}{\partial x^2}, \\ \frac{\partial C^{[1]}}{\partial t} = D_2 \frac{\partial^2 C^{[1]}}{\partial x^2}, \end{cases} \quad (11a)$$

$$\begin{cases} \frac{\partial T^{[2]}}{\partial t} = \alpha - (\beta + 1)T^{[2]}, \\ \frac{\partial C^{[2]}}{\partial t} = \beta T^{[2]}, \end{cases} \quad (11b)$$

$$\begin{cases} \frac{\partial T^{[3]}}{\partial t} = (T^{[3]})^2 C^{[3]}, \\ \frac{\partial C^{[3]}}{\partial t} = -(T^{[3]})^2 C^{[3]}. \end{cases} \quad (11c)$$

Equation (11a) is solved by first discretizing the PDE using a second-order finite-difference method. Then (11a) is converted to

$$\begin{cases} \frac{\partial T}{\partial t} = D_1 M_1 T, \\ \frac{\partial C}{\partial t} = D_2 M_2 C, \end{cases}$$

where M_1 and M_2 correspond to the finite difference stencil for $\frac{\partial^2 T}{\partial x^2}$ and $\frac{\partial^2 C}{\partial x^2}$ respectively. To solve (11c), we note that $\frac{\partial T^{[3]}}{\partial t} + \frac{\partial C^{[3]}}{\partial t} = 0$. Hence, $T^{[3]} + C^{[3]} = k$ for some constant k with respect to t . Substituting $C^{[3]} = k - T^{[3]}$ into the first equation of (11c), we can obtain a differential equation in $T^{[3]}$ only:

$$\frac{\partial T^{[3]}}{\partial t} = (T^{[3]})^2 (k - T^{[3]}). \quad (12)$$

Equation (12) can be solved using separation of variables and partial fraction decomposition. The exact solution of (11) is then given by

$$\begin{cases} T^{[1]}(t + \Delta t) = T^{[1]}(t) \exp(D_1 M_1 \Delta t), \\ C^{[1]}(t + \Delta t) = C^{[1]}(t) \exp(D_2 M_2 \Delta t), \end{cases} \quad (13a)$$

$$\begin{cases} T^{[2]}(t + \Delta t) = \frac{\exp(-\Delta t(\beta + 1))[T^{[2]}(t) - \alpha + T^{[2]}(t)\beta + \alpha \exp(\Delta t(\beta + 1))]}{\beta + 1}, \\ C^{[2]}(t + \Delta t) = C^{[2]}(t) + \frac{T^{[2]}(t)\beta + \alpha\beta\Delta t}{\beta + 1} \\ \quad - \frac{\beta \exp(-\Delta t(\beta + 1))[T^{[2]}(t) - \alpha + T^{[2]}(t)\beta + \alpha \exp(\Delta t(\beta + 1))]}{(\beta + 1)^2}, \end{cases} \quad (13b)$$

$$\begin{cases} \frac{1}{k^2} \ln \left| \frac{T^{[3]}(t + \Delta t)}{T^{[3]}(t + \Delta t) - k} \right| - \frac{1}{kT^{[3]}(t + \Delta t)} = \Delta t + c_1, \\ C^{[3]}(t + \Delta t) = k - T^{[3]}(t + \Delta t), \end{cases} \quad (13c)$$

where $c_1 = \frac{1}{k^2} \ln \left| \frac{T^{[3]}(t)}{T^{[3]}(t) - k} \right| - \frac{1}{kT^{[3]}(t)}$ and $k = T^{[3]}(t) + C^{[3]}(t)$.

We report on the performance using Strang, AK 3-2(i), OS 32-3(7), AK 3-2(ii), and AK 5-2 to solve (11) in sect. 4.1.

3.2 Plasma dynamics with kinetic Vlasov–Poisson equations

Plasmas have numerous applications in science and technology. For example, the manufacturing of integrated circuits relies on the plasma etching [15]. Plasma is also commonly used for electric propulsion [16]. Accordingly, it is important to understand the complicated phenomena that occur inside plasmas. The studies of plasmas rely heavily on numerical simulations because the equations that govern the plasma behavior generally have no analytical solution. The kinetic theory of the electrostatic collision-less plasmas is based on the Vlasov–Poisson system of equations [17, 18]. This system of equations provides a general description of plasma behavior under many conditions. However, the Vlasov equation is a PDE in six independent phase-space variables (three spatial co-ordinates and three velocities), and achieving an accurate solution for it in its full form is generally not feasible even for the most powerful supercomputers at present. Even simplified forms of the Vlasov equation can take several months to solve numerically. Therefore, any improvement in the computational performance that does not undermine the accuracy can significantly improve the effectiveness of simulations.

The electron cyclotron drift instability (ECDI) is a plasma instability that has recently received a lot of attention from the plasma science community [19, 20, 21, 22, 23, 24, 25, 26, 27]. In ECDI, the exponential growth of electric field energy is driven by the drift velocity of electrons with respect to ions in a magnetized warm plasma. It is well known that the ECDI fluctuations can lead to the electron anomalous current in plasmas and reduce the efficiency of the Hall thrusters. The details of this process, however, are not well understood. The ECDI is characterized by fast electron heating that leads to the appearance of high velocities and, as a result, a restrictive CFL condition.

Moreover, the wide scale of frequencies excited by this instability requires long simulation times, and a fine discretization in Fourier space is required to sufficiently resolve the ensuing large wavelengths. Satisfying all these requirements makes the simulations of the ECDI computationally expensive.

The behavior of the ECDI is governed by the Vlasov–Poisson system of equations. For one spatial dimension and two velocity dimensions (1D2V), these equations are

$$\frac{\partial f_e}{\partial t} + v_x \frac{\partial f_e}{\partial x} - \alpha_1 (E_x - v_z \alpha_2) \frac{\partial f_e}{\partial v_x} - \alpha_1 (\alpha_3 + v_x \alpha_2) \frac{\partial f_e}{\partial v_z} = 0, \quad (14a)$$

$$\frac{\partial f_i}{\partial t} + v_x \frac{\partial f_i}{\partial x} + E_x \frac{\partial f_i}{\partial v_x} = 0, \quad (14b)$$

$$\frac{\partial E_x}{\partial x} - \int_{-\infty}^{\infty} \int_{-\infty}^{\infty} f_i dv_x dv_z + \int_{-\infty}^{\infty} \int_{-\infty}^{\infty} f_e dv_x dv_z = 0, \quad (14c)$$

where the dependent variables $f_e = f_e(x, v_x, v_z, t)$ and $f_i = f_i(x, v_x, t)$ are distribution functions of the electrons and ions, respectively, $E_x = E_x(x, t)$ is the electric field, and α_1 , α_2 , and α_3 are parameters that depend on the ion mass, plasma density, and external fields. The total energy in this system is defined by

$$\begin{aligned} U(t) = & \frac{1}{2\alpha_1} \int_0^L \int_{-\infty}^{\infty} \int_{-\infty}^{\infty} (v_x^2 + v_z^2) f_e(x, v_x, v_z, t) dv_x dv_z dx + \frac{1}{2} \int_0^L \int_{-\infty}^{\infty} v_x^2 f_i(x, v_x, t) dv_x dx \\ & + \frac{1}{2} \int_0^L E_x^2 dx + \int_0^t \int_0^L \int_{-\infty}^{\infty} \int_{-\infty}^{\infty} \alpha_3 f_e(x, v_x, v_z, \tilde{t}) v_z dv_x dv_z dx d\tilde{t}, \end{aligned} \quad (15)$$

where L is the size of the physical domain. Here, we use a periodic boundary condition for the physical domain. For both f_e and f_i , we have

$$\lim_{v_x \rightarrow \pm\infty} f_s = 0, \quad \lim_{v_z \rightarrow \pm\infty} f_s = 0, \quad s = e, i. \quad (16)$$

These conditions mean that there can be no particle with an infinite velocity. Conditions (16) are imposed numerically by adjusting the boundaries so that $f_s \approx 10^{-8}$ in their vicinity.

A popular Eulerian–Vlasov numerical method is the *semi-Lagrangian* method [28, 29, 30, 31, 32, 33, 34, 35]. In this method, (14a) and (14b) are split into a number of sub-equations, and each sub-equation is integrated using the method of characteristics. For both the ions and electrons, the characteristic equations of the Vlasov equation are in the form of equations of particle motion. In this study, the semi-Lagrangian method, as discussed below, is used for the integration of the Vlasov–Poisson system.

We first consider the electron Vlasov equation (14a). For this equation, the characteristic equations are defined by

$$\frac{dX_e}{dt} = V_{X_e}, \quad (17a)$$

$$\frac{dV_{X_e}}{dt} = -\alpha_1(E_x(x, t) - V_{Z_e}\alpha_2), \quad (17b)$$

$$\frac{dV_{Z_e}}{dt} = -\alpha_1(\alpha_3 + V_{X_e}\alpha_2). \quad (17c)$$

Now, one can define characteristic curves

$$\mathbf{W}(t; x, v_x, v_z) \equiv (X_e(t; x, v_x, v_z), V_{X_e}(t; x, v_x, v_z), V_{Z_e}(t; x, v_x, v_z))$$

as functions that satisfy (17) and at time $t + \Delta t$ are terminated at the point (x, v_x, v_z) . From (14a) and (17), one can show that the distribution function is constant along the characteristic curves, i.e., $\left[\frac{df_e}{dt}\right]_{\mathbf{W}} = 0$, and accordingly,

$$f_e(x, v_x, v_z, t + \Delta t) = f_e(X_e(t; x, v_x, v_z), V_{X_e}(t; x, v_x, v_z), V_{Z_e}(t; x, v_x, v_z), t). \quad (18)$$

Therefore, for updating the solution of (14a) at $t + \Delta t$, one only needs to find the base of the characteristic curves $\mathbf{W}(t; x, v_x, v_z)$. In general, to find the base of the characteristic curve, one needs to perform a backward integration. Because of this, the $\mathbf{W}(t; x, v_x, v_z)$ is in general found implicitly by solving a nonlinear equation $\mathbf{F}(\mathbf{W}(t; x, v_x, v_z), E_x(t)) = \mathbf{0}$ [36, 37]. However, this particular problem can be solved by splitting the Vlasov equation into equations along the directions of one of the independent variables at a time. For example, (14a) is split into three sub-equations

$$\frac{\partial f_e^{[1]}}{\partial t} + v_x \frac{\partial f_e^{[1]}}{\partial x} = 0, \quad (19a)$$

$$\frac{\partial f_e^{[2]}}{\partial t} + a_z \frac{\partial f_e^{[2]}}{\partial v_z} = 0, \quad (19b)$$

$$\frac{\partial f_e^{[3]}}{\partial t} + a_x \frac{\partial f_e^{[3]}}{\partial v_x} = 0, \quad (19c)$$

where $a_z \equiv -\alpha_1(\alpha_3 + v_x\alpha_2)$ and $a_x \equiv -\alpha_1(E_x - v_z\alpha_2)$. In (19a), the coefficient of $\frac{\partial f_e^{[1]}}{\partial x}$ is v_x , which is a constant of that equation. Similarly in (19b) and (19c), a_x and a_z are constant. Because of this property of (19), the exact base of the characteristic of these equations can be found explicitly. Using the method of characteristics, solutions of (19) at $t + \Delta t$ are

$$f_e^{[1]}(x, t + \Delta t) = f_e^{[1]}(x - v_x\Delta t), \quad (20a)$$

$$f_e^{[2]}(v_z, t + \Delta t) = f_e^{[2]}(v_z - a_z \Delta t), \quad (20b)$$

$$f_e^{[3]}(v_x, t + \Delta t) = f_e^{[3]}(v_x - a_x \Delta t). \quad (20c)$$

We note that (20) are the exact solutions of (19). However, because at time t , f_e is only known at a particular grid point (x_n, v_{xn}, v_{zn}) , evaluating (20) requires an interpolation. Many interpolation methods are suggested in the literature; among them, the cubic spline is one of the most popular because it is believed to keep a good balance between the accuracy and the performance in semi-Lagrangian methods [38]. In this study, all the interpolations are done using cubic splines.

Similar to (14a), (14b) is split into two equations

$$\frac{\partial f_i^{[1]}}{\partial t} + v_x \frac{\partial f_i^{[1]}}{\partial x} = 0, \quad (21a)$$

$$\frac{\partial f_i^{[2]}}{\partial t} + E_x \frac{\partial f_i^{[2]}}{\partial v_x} = 0, \quad (21b)$$

which are solved using the method of characteristics

$$f_i^{[1]}(x, t + \Delta t) = f_i^{[1]}(x - v_x \Delta t), \quad (22a)$$

$$f_i^{[2]}(v_x, t + \Delta t) = f_i^{[2]}(v_x - E_x \Delta t). \quad (22b)$$

Although (14b) is split into two operators, we cast it as a 3-splitting method with a trivial operator [3], i.e., a trivial operator in the v_z direction. Equation (14) can then split into the following three operators:

$$\begin{cases} \frac{\partial f_e^{[1]}}{\partial t} = -v_x \frac{\partial f_e^{[1]}}{\partial x}, \\ \frac{\partial f_i^{[1]}}{\partial t} = -v_x \frac{\partial f_i^{[1]}}{\partial x}, \end{cases} \quad (23a)$$

$$\begin{cases} \frac{\partial f_e^{[2]}}{\partial t} = -a_z \frac{\partial f_e^{[2]}}{\partial v_z}, \end{cases} \quad (23b)$$

$$\begin{cases} \frac{\partial f_e^{[3]}}{\partial t} = -a_x \frac{\partial f_e^{[3]}}{\partial v_x}, \\ \frac{\partial f_i^{[3]}}{\partial t} = -E_x \frac{\partial f_i^{[3]}}{\partial v_x}. \end{cases} \quad (23c)$$

The split Vlasov equations (23) are predominantly solved using the Strang splitting method (4) for three operators. Equation (14c) is integrated after the first stage α_1 of the operator-splitting process.

We note that the energy $U(t)$ defined by (15) is theoretically constant. However, the semi-Lagrangian method is not energy conserving. Because of

this, the so-called phenomena of “numerical heating” and “numerical cooling” are concerns in semi-Lagrangian simulations. Accordingly, the deviation from energy conservation is a reasonable indicator of simulation error. This is especially true when qualitative global aspects of the solution are of interest more so than specific local values.

For this problem, we test another splitting method AK 3-2(i) in addition to the Strang method. Equation (14c) is again integrated after the first stage α_1 . We note that the AK 3-2(i) method has one more sub-integration compared to the Strang method. Accordingly, it generally has a great computational expense on a per step basis. In order for AK 3-2(i) to outperform Strang, therefore, it must allow for an increased step size that more than offsets this additional cost per step while maintaining sufficient accuracy.

4 Results

In this section, we describe the results from applying a number of second-order, 3-splitting methods to the Brusselator and ECDI problems. We find that some alternatives to traditional Strang 3-splitting can be 10%–20% more efficient for a given level of accuracy.

4.1 Brusselator

A reference solution for the Brusselator problem (10) for $t \in [0, 80]$ is computed using the MATLAB parabolic and elliptic PDE solver `pdepe`. We decreased the spatial meshsize Δx and adjusted the absolute and relative tolerances for the solver until there were at least 6 matching digits between successive approximations at 32,000 and 800 uniformly distributed points in space and time, respectively. For our experiments with the various splitting methods, the spatial derivatives are discretized using central finite differences on a uniform grid on the interval $x \in [0, 1]$.

The numerical experiments using operator-splitting methods are implemented using Python. Although all subintegrators have analytical solutions, the solution (13a) requires the matrix exponential, and the solution (13c) requires the solution to a non-linear equation. It turns out to be faster to obtain an “exact” solution by solving (11a) and (11c) with the Python `scipy.integrate.solve_ivp` function using `rtol = 1e-10` and `atol = 1e-13` and using the closed-form for (11b).

In this example, the error in the numerical solution of a quantity X is measured using the mixed root mean square (MRMS) error defined by

$$\text{error} = [\text{MRMS}]_X = \sqrt{\frac{1}{N} \sum_{i=1}^N \left(\frac{X_i^{\text{ref}} - X_i}{1 + \text{abs}(X_i^{\text{ref}})} \right)^2},$$

where X_i^{ref} and X_i , respectively, denote the reference solution and the numerical solution at $t_f = 80$ at spatial point i sampled at $N = 101$ equally spaced

points on the interval $[0, 1]$. The order of convergence p of the numerical solution was then computed in the standard way as

$$p = \frac{\log(\text{error}_1/\text{error}_2)}{\log(\Delta t_1/\Delta t_2)},$$

where the subscripts 1 and 2 refer to computations performed using time steps Δt_1 and Δt_2 . Fig. 1 shows second-order convergence is observed for all of Strang, AK 3-2(i), OS 32-3(7), AK 3-2(ii), and AK 5-2. The number in the square bracket represents the number of sub-integrations needed for each method. From the figure, we see that the alternatives to Strang have similar (and better) accuracy for a given step size. However, they all involve a greater number of sub-integrations and hence are generally more computationally expensive per step.

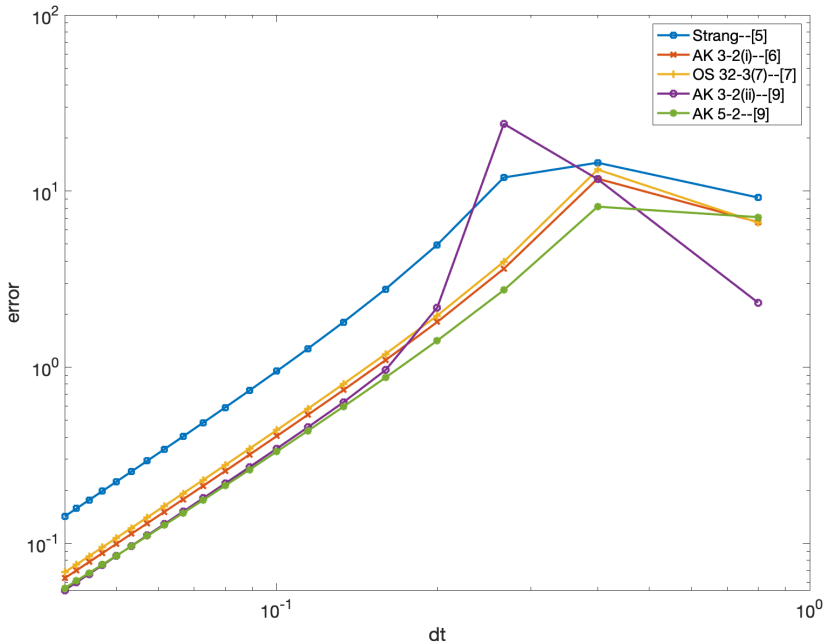


Fig. 1 Convergence of second-order splitting methods. All methods demonstrate the expected convergence rate.

Remark 1 The relative sizes of experimental errors observed using Strang, AK 3-2(i), OS 32-3(7), AK 3-2(ii), and AK 5-2 do not strictly reflect the relative sizes of the LEMs presented in table 1. This is not a surprise because the LEM is only a coarse measure of the size of the coefficients that make up the local truncation error. In

[9], the authors observed a smaller error using AK 3-2(ii) compared to AK 5-2 when applied to the Vlasov–Maxwell system.

We further note by rearranging the order of the operators, there are 6 different versions of Strang 3-splitting (4). All require 5 sub-integrations and have similar LEM. However, the cost of solving each sub-integrator is different, and the actual error of each of version is different. We consider the following two versions: Strang(2-3-1), whose coefficients are given in table 6 and uses only one evaluation of the most time-consuming operator, the diffusion operator acting on $T^{[1]}$ and $C^{[1]}$, and Strang(1-3-2), whose coefficients are given in table 7 and generally has the smallest actual error for a given step size Δt for this problem.

Taking into consideration the number of sub-integrations and the size of the error produced, one may hypothesize that only AK 3-2(i) is competitive versus Strang for this problem, and informal numerical experiments with all the methods support this hypothesis. Accordingly, we report on the efficiency comparisons only between Strang(2-3-1), Strang(1-3-2), and AK 3-2(i).

k	$\alpha_1^{[k]}$	$\alpha_2^{[k]}$	$\alpha_3^{[k]}$
1	0	0.5	0.5
2	1	0	0.5
3	0	0.5	0

Table 6 Operator-splitting coefficients of Strang(2-3-1).

k	$\alpha_1^{[k]}$	$\alpha_2^{[k]}$	$\alpha_3^{[k]}$
1	0.5	0	0.5
2	0	1	0.5
3	0.5	0	0

Table 7 Operator-splitting coefficients of Strang(1-3-2).

To compare the efficiency of Strang(2-3-1), Strang(1-3-2), and AK 3-2(i), we determine the largest possible step size Δt can be used for each method to achieve MRMS errors of 5%, 4%, 3%, 2%, 1%, and 0.5%. For each MRMS level, we record the minimum wall-clock time needed to perform the Strang(2-3-1), Strang(1-3-2), and AK 3-2(i) over 10 runs. The efficiency tests are performed on a Quad-core Intel Xeon Gold 5122 CPU 3.60GHz with 48GB of RAM running Ubuntu 18.04 LTS. We observed that Strang(2-3-1) is more efficient than Strang(1-3-2) because it evaluates the most expensive sub-integration only once, and its accuracy level is comparable to Strang(1-3-2). In table 8, we present the detailed comparison between Strang(2-3-1) and AK 3-2(i) at various MRMS levels. We notice that AK 3-2(i) is on average 9% – 11% more efficient than Strang(2-3-1).

MRMS (%)	AK 3-2(i)		Strang(2-3-1)		Time saved (%)
	Δt	CPU (s)	Δt	CPU (s)	
5	0.300751880	34.7206	0.214477212	38.4495	9.698175529
4	0.275862069	35.1449	0.197530864	38.7529	9.310270973
3	0.246913580	35.1634	0.176991150	39.6837	11.39082293
2	0.208333333	35.7434	0.149532710	40.0799	10.81963777
1	0.153256705	37.718	0.110041265	41.5642	9.253636543
0.5	0.110497238	40.0803	0.079522863	44.0782	9.070016471

Table 8 Comparison of wall-clock time needed by Strang(2-3-1) and AK 3-2(i) at various accuracy levels.

4.2 Plasma dynamics with kinetic Vlasov–Poisson equations

Our code is implemented in Fortran 90. Some details of this implementation can be found in [37]. The parameters used for the ECDI simulations are listed in table 9. The values of α_1 , α_2 , and α_3 correspond to the typical operation regime of Hall thrusters and are also used in [25, 27, 26]. Also in this table, N_x is the number of cells in the x -direction of the both ion and electron distribution grids; $N_{v_{xe}}$ and $N_{v_{ze}}$ are the number of cells in the v_x - and v_z -directions of the electron grid, respectively; and $N_{v_{xi}}$ is the number of cells in the v_x -direction of the ion grid. We note that because the ions are much heavier than the electrons, their velocity often remains much smaller than that of the electrons during the simulation. Because of this, (14b) is usually solved on a much coarser grid than (14a).

Parameter	Value
α_1	2.39×10^5
α_2	4.03×10^{-4}
α_3	0.1487
N_x	2048
$N_{v_{xe}}$	1200
$N_{v_{ze}}$	1200
$N_{v_{xi}}$	200
L	600

Table 9 Parameters used for the ECDI simulation.

At the initial stage of the ECDI, called the linear regime, E_x grows exponentially with time. For this growth, different Fourier harmonics of E_x show different time exponents. These exponents are referred to as the “linear growth rates”. The linear growth rates can be calculated analytically by solving a nonlinear algebraic equation that is derived by applying perturbation methods to the Vlasov–Poisson system. The details of this derivation can be found in [39], and a numerical method for solving the nonlinear algebraic equation is discussed in [40]. The linear growth rates can be also measured from the simulations, and the results of these measurements can be used as a measure of the accuracy of the simulations [41, 42, 27]. Fig. 2 compares the analytical linear growth rates with the growth rates that are measured numerically

by different splitting methods. We can see that, in all cases, the measured growth rates remain close to each other and the analytical growth rates. This means that although both the Strang and the AK 3-2(i) methods provide a reasonable accuracy of the linear regime, the linear growth rates (and accordingly the short-time behavior of ECDI) do not provide a suitable measure for distinguishing the accuracy of these methods.

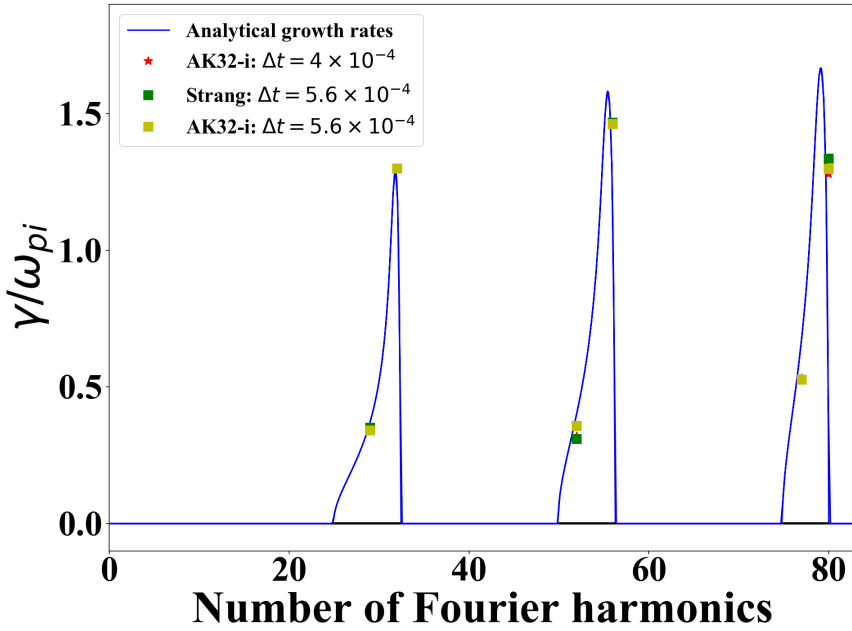


Fig. 2 The linear growth rates of the Strang and AK 3-2(i) methods.

The linear regime of the instability is followed in time by the nonlinear regime. In contrast to the linear regime, analysis of the nonlinear regime is generally performed through simulation. For comparing the accuracy of different methods, we use the maximum deviation from energy conservation as a measure of the error of the simulations. This measure is defined by

$$\Delta_t U = \left| \frac{U(t) - U(0)}{U(0)} \right| \times 100.$$

Because the $\Delta_t U$ is a function of time, its temporal value might not be a consistent metric for comparing two competing splitting schemes. Nevertheless, in most applications, a maximum deviation of energy conservation can be tolerated, e.g., 2%. Here, although we show the temporal evolution of $\Delta_t U$, we use the maximum of $\Delta_t U$ over time as a metric to determine solution accuracy.

Fig. 3 shows the $\Delta_t U$ for the Strang and the AK 3-2(i) methods. In this figure, the simulation duration is 70, which approximately corresponds to the $2 \mu\text{s}$ timespan considered in the previous studies [27, 25, 26, 43]. We can see that the maximum error is the lowest in AK 3-2(i) with $\Delta t = 4 \times 10^{-4}$. The Strang method with $\Delta t = 4 \times 10^{-4}$ has about the same maximum error as the AK 3-2(i) with a time step that is 40% larger ($\Delta t = 5.6 \times 10^{-4}$). This means that for $\delta \approx 1.4$ in (9). However, when the time step of the Strang method is increased by 40% to $\Delta t = 5.6 \times 10^{-4}$, the error jumps to about 7%.

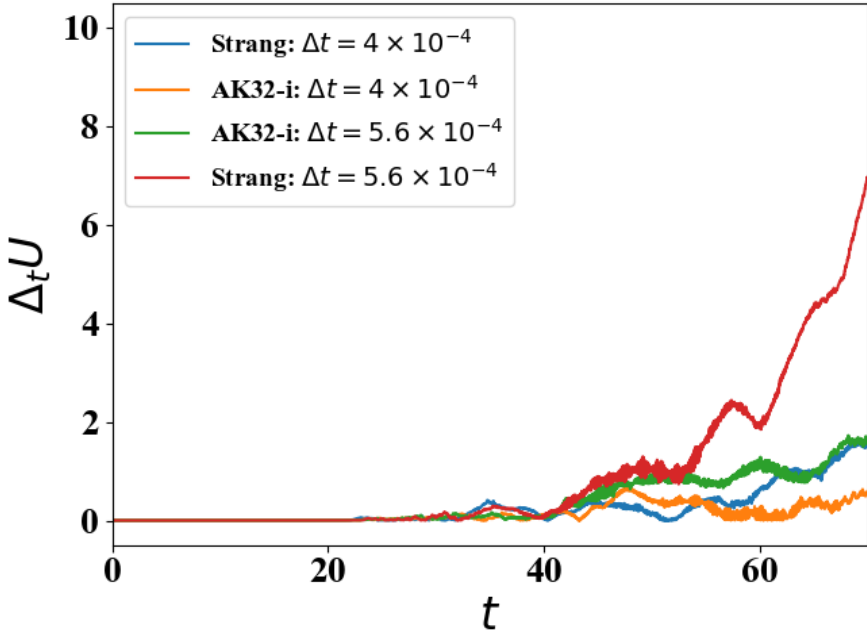


Fig. 3 Maximum deviation from energy conservation of the Strang and AK 3-2(i) methods.

For calculating the efficiency gain η from (9), we also calculated the extra-time-fraction Γ . Compared with Strang, the AK 3-2(i) method needs to evaluate one extra step of (19c) and (21b). Therefore, one can assume $\tilde{\tau}_{(19c)}^{AK3-2(i)}$ and $\tilde{\tau}_{(21b)}^{AK3-2(i)}$. The results of our measurements of Γ are shown in table 10 for different sub-integrators of the ECDCI. We note that, because the electron grid is much finer than that of the ions ($\Gamma_{v_{xe}} \gg \Gamma_{v_{xi}}$), we can neglect $\Gamma_{v_{xi}}$ arising from (21b). Accordingly, $\Gamma \approx 0.15 - 0.2$, which, using (9) and (8), leads to an efficiency gain of 14% to 18% of the AK 3-2(i) with respect to Strang. These estimates are consistent with experimental observations.

Sub-integrator of	$\Gamma \times 100$
(19a)	5 – 7
(19b)	18 – 20
(19c)	15 – 20
(21a)	0.003 – 0.3
(21b)	0.2 – 0.6
(14c)	15 – 25

Table 10 The extra-time-fractions Γ for different sub-integrators of the ECDI operators. Measurement performed using 1 to 40 processors and on various computers.

5 Discussion and Conclusions

Operator splitting is popular in the numerical solution of differential equations. The most common framework for splitting is into two parts; however, there can be advantages to being able to split a given problem into three parts. The generalization of Strang splitting to three operators is arguably the most popular 3-splitting method. Although alternatives to Strang exist, they are less well known. In this paper, we test some alternative 3-splitting methods on two applications, the Brusselator and ECDI problems. We demonstrate worthwhile (10%–20%) improvements in efficiency over traditional Strang splitting, potentially shaving days of computing time off of real problems that require weeks to simulate (or weeks off of problems that require months).

In the experiments of the Brusselator problem, we examined various second-order accurate 3-splitting methods and concluded that AK 3-2(i) is the most efficient method based on overall computation time. Our experiments have taken into account the LEM error, the number sub-integrations, and the cost of each sub-integration. We observe that although all 6 versions of the Strang method exhibit similar accuracy and require the same number of sub-integrations, Strang(2-3-1) is the most efficient among the 6 versions because the accuracy is among the best and the most expensive operator [1] is evaluated only once. We further note that a splitting method may have an optimum LEM error but may require many splitting stages and sub-integrations to solve one time step. These additional costs may ultimately offset the efficiency gained from the minimized error. Therefore, when choosing an efficient operator-splitting method, we seek to balance the error and the number of sub-integrations required. This balanced approach is essential not only to 3-splitting problems but also to general N-splitting problems. Furthermore, we echo the result in [7] that for some test problems, such as the Gray–Scott equations or the Brusselator equations, we may not experience efficiency gain by splitting the differential equations into 3 operators as opposed to 2 operators. The potential advantage is that by splitting into 3 operators, some of the sub-integrators admit a closed-form solution, which can potentially be efficiently evaluated.

In the full Vlasov–Poisson equation in 6-dimensional phase space, one can apply splitting to each direction, and therefore, six operators need to be solved [44]. Due to their extreme computational cost, such simulations are generally not feasible at present. Here, we applied a 3-splitting to a simplified version of

the Vlasov–Poisson system in one spatial direction and two velocity directions. The 3-splitting helped us to calculate the base of the characteristic equations explicitly. We also tried a 2-splitting version of the code, in which the two velocity directions are treated as only one (rotation) operator. This rotation operator is then integrated using the method of characteristics, which requires a 2-dimensional B-spline cubic interpolation [37]. For the ECDI problem, we observed that the overall performance deteriorated compared to the 3-splitting approach. In [9], a new splitting scheme is proposed for the exact integration of the rotation operator. Applying the new method to the Vlasov–Maxwell system, the authors observed a significant increase in the performance compared to the 2-dimensional spectral interpolation. Therefore, we hypothesize that this method can also help increase the performance of our 2-splitting code and propose the investigation of its impact on the ECDI problem as future work.

In the ECDI problem, we measured $\delta \approx 1.4$ and $\Gamma \approx 0.15 - 0.2$, which led to 15% to 20% efficiency gain. This efficiency gain allowed a simulation using 32 processors to complete in about 8 days using AK 3-2(i) versus about 10 days using Strang. We have performed other simulations using a simulation domain 4 times larger than that in this work that took about 2 months [45]. In general, 2- and 3-dimensional Vlasov simulations can easily take several months even using hundreds or thousands of processors [46, 44]. Therefore, the perhaps modest-looking efficiency gain provided by the AK 3-2(i) method can lead to several weeks of real time saved for running these simulations.

To examine the effect of the resolution on δ and Γ , we repeated the simulation with the AK 3-2(i) method for the $N_{v_{xe}}$ between 800 to 1200 and observed that these quantities did not significantly change. Similarly, simulations with up to 40 cores did not have a significant impact on Γ . We do not expect that the parallelization or the number of cores to have a significant impact on δ because this quantity only depends on the accuracy of a splitting method and not on the number of cores used.

Other than AK 3-2(i), we tried other 3-splitting methods, namely AK 3-2(ii), AK 5-2, and AK 11-4, for the ECDI problem. The general conclusion from these experiments is that none of these methods are likely to be competitive with Strang in terms of efficiency. The AK 3-2(ii) and AK 5-2 have four more sub-integrators than Strang, but they approximately gave the same $\Delta_t U$ as Strang for the same $\Delta t = 4 \times 10^{-4}$. Also, the AK 11-4 is a fourth-order splitting method with 16 sub-integrators more than Strang. Applying AK11-4 on the ECDI problem and using the values of Γ in table 10, we calculate that this method is at least 3 times more expensive per time step than Strang. However, our experiment with $\Delta t = 3 \times 4 \times 10^{-4}$ showed a much larger error than Strang with $\Delta t = 4 \times 10^{-4}$. This may be explained by the fact that the sub-integrators of our code are based on cubic spline interpolation, and the error may overshadow the splitting error of a fourth-order method. Addressing the efficiency of the splitting methods when higher-order interpolation methods are used is beyond the scope of the current study.

Acknowledgments. The authors gratefully acknowledge funding from the Natural Sciences and Engineering Research Council of Canada under its Discovery Grant Program (RGPN 2020-04467 (RJS) and RGPN 2022-04482 (AS)) as well as from the US Air Force Office of Scientific Research FA9550-21-1-0031 (AS). A. Tavassoli acknowledges the support of Dr. Magdi Shoucri in developing the semi-Lagrangian code.

Statements and Declarations

The authors have no conflict of interest nor competing interests to declare that are relevant to the content of this article.

References

- [1] Ascher, U.M., Ruuth, S.J., Spiteri, R.J.: Implicit-explicit Runge–Kutta Methods for Time-dependent Partial Differential Equations. *Appl. Numer. Math.* **25**(2-3), 151–167 (1997)
- [2] Lefever, R., Nicolis, G.: Chemical instabilities and sustained oscillations. *Journal of Theoretical Biology* **30**(2), 267–284 (1971). [https://doi.org/10.1016/0022-5193\(71\)90054-3](https://doi.org/10.1016/0022-5193(71)90054-3)
- [3] Strang, G.: On the construction and comparison of difference schemes. *SIAM Journal on Numerical Analysis* **5**(3), 506–517 (1968)
- [4] Marchuk, G.I.: On the theory of the splitting-up method. In: Hubbard, B. (ed.) *Numerical Solution of Partial Differential equations–II*, pp. 469–500. Academic Press, London (1971)
- [5] Auzinger, W., Hofstätter, H., Ketcheson, D., Koch, O.: Practical splitting methods for the adaptive integration of nonlinear evolution equations. Part I: Construction of optimized schemes and pairs of schemes. *BIT Numerical Mathematics* **57**(1), 55–74 (2017)
- [6] Auzinger, W.: Coefficients of various splitting methods. <http://www.asc.tuwien.ac.at/~winfried/splitting/>
- [7] Auzinger, W., Koch, O., Quell, M.: Adaptive high-order splitting methods for systems of nonlinear evolution equations with periodic boundary conditions. *Numer. Algorithms* **75**(1), 261–283 (2017). <https://doi.org/10.1007/s11075-016-0206-8>
- [8] Crouseilles, N., Einkemmer, L., Faou, E.: Hamiltonian splitting for the Vlasov–Maxwell equations. *Journal of Computational Physics* **283**, 224–240 (2015)
- [9] Bernier, J., Casas, F., Crouseilles, N.: Splitting methods for rotations: application to Vlasov equations. *SIAM J. Sci. Comput.* **42**(2), 666–697 (2020). <https://doi.org/10.1137/19M1273918>
- [10] Hairer, E., Wanner, G., Lubich, C.: *Geometric numerical integration: structure-preserving algorithms for ordinary differential equations* vol. 31. Springer, Heidelberg (2006)

22 REFERENCES

- [11] Auzinger, W., Herfort, W.: Local error structures and order conditions in terms of Lie elements for exponential splitting schemes. *Opuscula Mathematica* **34**(2), 243–255 (2014)
- [12] Bernier, J., Casas, F., Crouseilles, N.: Splitting methods for rotations: application to Vlasov equations. *SIAM Journal on Scientific Computing* **42**(2), 666–697 (2020)
- [13] Casas, F., Escorihuela-Tomás, A.: Composition methods for dynamical systems separable into three parts. *Mathematics* **8**(4), 533 (2020)
- [14] Ropp, D.L., Shadid, J.N.: Stability of operator splitting methods for systems with indefinite operators: reaction-diffusion systems. *Journal of Computational Physics* **203**(2), 449–466 (2005)
- [15] Donnelly, V.M., Kornblit, A.: Plasma etching: Yesterday, today, and tomorrow. *Journal of Vacuum Science & Technology A: Vacuum, Surfaces, and Films* **31**(5), 050825 (2013)
- [16] Lev, D., Myers, R.M., Lemmer, K.M., Kolbeck, J., Koizumi, H., Polzin, K.: The technological and commercial expansion of electric propulsion. *Acta Astronautica* **159**, 213–227 (2019)
- [17] Nicholson, D.R., Nicholson, D.R.: Introduction to plasma theory. Wiley, New York (1983)
- [18] Chen, F.F.: Introduction to plasma physics and controlled fusion, 3rd edn. Springer, Switzerland (2016)
- [19] Boeuf, J.-P., Garrigues, L.: $E \times B$ electron drift instability in Hall thrusters: Particle-in-cell simulations vs. theory. *Physics of Plasmas* **25**(6), 061204 (2018)
- [20] Charoy, T., Lafleur, T., Laguna, A.A., Bourdon, A., Chabert, P.: The interaction between ion transit-time and electron drift instabilities and their effect on anomalous electron transport in Hall thrusters. *Plasma Sources Science and Technology* **30**(6), 065017 (2021)
- [21] Sengupta, M., Smolyakov, A.: Mode transitions in nonlinear evolution of the electron drift instability in a 2D annular $E \times B$ system. *Physics of Plasmas* **27**(2), 022309 (2020)
- [22] Asadi, Z., Taccogna, F., Sharifian, M.: Numerical study of electron cyclotron drift instability: Application to Hall thruster. *Frontiers in Physics* **7**, 140 (2019)
- [23] Hara, K., Tsikata, S.: Cross-field electron diffusion due to the coupling of drift-driven microinstabilities. *Physical Review E* **102**(2), 023202 (2020)
- [24] Mandal, D., Elskens, Y., Lemoine, N., Doveil, F.: Cross-field chaotic transport of electrons by $E \times B$ electron drift instability in Hall thruster. *Physics of Plasmas* **27**(3), 032301 (2020)
- [25] Janhunen, S., Smolyakov, A., Chapurin, O., Sydorenko, D., Kaganovich, I., Raitses, Y.: Nonlinear structures and anomalous transport in partially magnetized $E \times B$ plasmas. *Physics of Plasmas* **25**(1), 011608 (2018)
- [26] Janhunen, S., Smolyakov, A., Sydorenko, D., Jimenez, M., Kaganovich, I., Raitses, Y.: Evolution of the electron cyclotron drift instability in two-dimensions. *Physics of Plasmas* **25**(8), 082308 (2018)

- [27] Tavassoli, A., Smolyakov, A., Shoucri, M., Spiteri, R.J.: Nonlinear regimes of the electron cyclotron drift instability in Vlasov simulations. *Physics of Plasmas* **29**(3), 030701 (2022)
- [28] Cheng, C.-Z., Knorr, G.: The integration of the Vlasov equation in configuration space. *Journal of Computational Physics* **22**(3), 330–351 (1976)
- [29] Cheng, C.: The integration of the Vlasov equation for a magnetized plasma. *Journal of Computational Physics* **24**(4), 348–360 (1977)
- [30] Sonnendrücker, E., Roche, J., Bertrand, P., Ghizzo, A.: The semi-Lagrangian method for the numerical resolution of the Vlasov equation. *Journal of Computational Physics* **149**(2), 201–220 (1999)
- [31] Crouseilles, N., Mehrenberger, M., Sonnendrücker, E.: Conservative semi-Lagrangian schemes for Vlasov equations. *Journal of Computational Physics* **229**(6), 1927–1953 (2010)
- [32] Crouseilles, N., Respaud, T., Sonnendrücker, E.: A forward semi-Lagrangian method for the numerical solution of the Vlasov equation. *Computer Physics Communications* **180**(10), 1730–1745 (2009)
- [33] Qiu, J.-M., Christlieb, A.: A conservative high order semi-Lagrangian WENO method for the Vlasov equation. *Journal of Computational Physics* **229**(4), 1130–1149 (2010)
- [34] Besse, N., Mehrenberger, M.: Convergence of classes of high-order semi-Lagrangian schemes for the Vlasov–Poisson system. *Mathematics of computation* **77**(261), 93–123 (2008)
- [35] Ghizzo, A., Huot, F., Bertrand, P.: A non-periodic 2D semi-Lagrangian Vlasov code for laser–plasma interaction on parallel computer. *Journal of Computational Physics* **186**(1), 47–69 (2003)
- [36] Coulaud, O., Sonnendrücker, E., Dillon, E., Bertrand, P., Ghizzo, A.: Parallelization of semi-Lagrangian Vlasov codes. *Journal of Plasma Physics* **61**(3), 435–448 (1999)
- [37] Shoucri, M.: The method of characteristics for the numerical solution of hyperbolic differential equations. In: Baswell, A.R. (ed.) *Advances in Mathematics Research*, Volume 8, pp. 1–87. Nova Science Publishers, Inc., New York (2009). Chap. 1
- [38] Staniforth, A., Côté, J.: Semi-Lagrangian integration schemes for atmospheric models—A review. *Monthly weather review* **119**(9), 2206–2223 (1991)
- [39] Gary, S.P.: *Theory of space plasma microinstabilities vol. 7*. Cambridge University Press, Cambridge (1993)
- [40] Cavalier, J., Lemoine, N., Bonhomme, G., Tsikata, S., Honore, C., Gresillon, D.: Hall thruster plasma fluctuations identified as the $E \times B$ electron drift instability: Modeling and fitting on experimental data. *Physics of Plasmas* **20**(8), 082107 (2013)
- [41] Tavassoli, A., Chapurin, O., Jimenez, M., Papahn Zadeh, M., Zintel, T., Sengupta, M., Couëdel, L., Spiteri, R.J., Shoucri, M., Smolyakov, A.: The role of noise in PIC and Vlasov simulations of the Buneman instability.

- Physics of Plasmas **28**(12), 122105 (2021)
- [42] Tavassoli, A., Shoucri, M., Smolyakov, A., Papahn Zadeh, M., Spiteri, R.J.: Backward waves in the nonlinear regime of the Buneman instability. Physics of Plasmas **28**(2), 022307 (2021)
 - [43] Lafleur, T., Baalrud, S., Chabert, P.: Theory for the anomalous electron transport in Hall effect thrusters. I. Insights from particle-in-cell simulations. Physics of Plasmas **23**(5), 053502 (2016)
 - [44] Kormann, K., Reuter, K., Rampp, M.: A massively parallel semi-Lagrangian solver for the six-dimensional Vlasov–Poisson equation. The International Journal of High Performance Computing Applications **33**(5), 924–947 (2019)
 - [45] Tavassoli, A., Zadeh, M.P., Smolyakov, A., Shoucri, M., Spiteri, R.J.: The electron cyclotron drift instability: a comparison of particle-in-cell and continuum Vlasov simulations. arXiv preprint arXiv:2211.05892 (2022)
 - [46] Tanaka, S., Yoshikawa, K., Minoshima, T., Yoshida, N.: Multidimensional Vlasov–Poisson simulations with high-order monotonicity- and positivity-preserving schemes. The Astrophysical Journal **849**(2), 76 (2017)